



The potential of elastic/polarization lidars to retrieve extinction profiles

Elina Giannakaki^{1,2}, Panos Kokkalis^{3,4}, Eleni Marinou^{4,5}, Nikolaos S. Bartsotas⁶, Vassilis Amiridis⁴, Albert Ansmann⁷, Mika Komppula²

5 ¹Department of Environmental Physics and Meteorology, University of Athens, Athens, 15784, Greece

²Finnish Meteorological Institute, Atmospheric Research Centre of Eastern Finland, Kuopio, 70211, Finland

³Physics Department, Faculty of Science, Kuwait University, Kuwait

⁴Institute for Astronomy, Astrophysics, Space Applications and Remote Sensing, National Observatory of Athens, Athens 15236, Greece

10 ⁵Institute of Atmospheric Physics, German Aerospace Center (DLR), Oberpfaffenhofen, 82234, Germany

⁶Atmospheric Modeling and Weather Forecasting Group, Department of Physics, National and Kapodistrian University of Athens, Greece

⁷Leibniz Institute for Tropospheric Research (TROPOS), Leipzig, 04318, Germany

15

Correspondence to: Elina Giannakaki (elina@phys.uoa.gr)

20

Abstract. In this study we estimate the particle extinction profiles at Finokalia, Crete, using only the information provided by the elastic and polarization channels of a Polly^{XT} lidar system. Most of the time Finokalia site is affected by only two aerosol types, i.e. marine and dust particles. These two aerosol types, having different optical properties, permit the separation of aerosol mixture. The proposed method uses the particle backscatter profiles at 532 nm and the vertically resolved particle linear depolarization ratio measurements at the same wavelength. The particle linear depolarization ratio and the lidar ratio values of pure aerosol types are taken from literature. The total extinction profile is then estimated and compared well with Raman retrievals. Any difference between the proposed methodology and Raman extinction profiles indicates that the non-dust component could be probably attributed to polluted marine or polluted continental aerosols. Comparison with sun-photometric aerosol optical depth observations is performed as well during daytime with reasonable differences between the two instruments. Differences in the total aerosol optical depth is attributed to the limited ability of the lidar to correctly represent the aerosol optical properties in the near range due to overlap problem.

25

1 Introduction

30

Aerosols play an important role in the atmospheric radiation budget (IPCC, 2013). Depending on the aerosol type, they can absorb or scatter the incoming and outgoing radiation, warming or cooling the atmosphere and depending on their size and



composition, they can act as condensation nuclei, modifying cloud physical and radiative properties (Kauffman et al., 2002). However, climate forcing by tropospheric aerosols remain one of the largest uncertainties in climate variability and climate change studies. The types of aerosols can be categorized roughly as mineral dust, sea salt, volcanic, carbonaceous, or sulfate aerosols originating from various natural and anthropogenic sources.

35 Several lidar studies have revealed that a broad variety of aerosol mixtures is occurred in the European continent (Balis et al., 2004, Papayannis et al. 2005). The mixing occurs because of the relatively long pathways of air masses across different aerosol source regions before the detection over European continent. For example, Saharan dust observed in South Europe is often already lifted over Africa to heights above 1-2 km, so that mixing with marine particles is almost prohibited. Sea-salt particles are near spherical and non-absorbing, whereas dust particles are non-spherical and show considerable absorption. Thus mixing

40 of either marine aerosol or absorbing aerosol or both with dust particles may result to different optical properties. The measured optical properties is then resulted from the contribution of each aerosol type to the total aerosol load. Lidar measurements provide vertical profiling of various particle properties with high spatial and temporal resolution, and based on the optical properties the identification of different aerosol types becomes feasible. The determination of the extinction-to-backscatter ratio (the so-called lidar ratio) profile is possible using the Raman-lidar technique (Ansmann, 1992).

45 The lidar ratio contains information on the aerosol type, since it depends on the index of refraction and on the size of particles. Many studies have demonstrated that the lidar ratio is a quantity valuable for aerosol characterization (Ansmann et al., 2002; Müller et al., 2007; Mattis et al., 2004; Amiridis et al., 2005; Giannakaki et al., 2010, Giannakaki et al., 2016; Groß et al, 2011; Groß et al, 2013; Groß et al, 2015). However, the majority of aerosol lidars, including the recently launched Cloud-Aerosol Lidar and Pathfinder Satellite Observations (CALIPSO) lidar are so-called elastic-backscatter lidars. Such lidars allow us to

50 retrieve only the particle backscatter coefficient (Klett, 1981). Elastic backscatter lidars are often equipped with polarization measurements. Recently, the polarization lidar technique has been additionally used to separate the desert dust aerosol component from other aerosol components (Tesche et al., 2009). Desert dust causes high depolarization of backscattered light, whereas typical non-desert aerosol mixtures, like marine aerosols, lead to very low depolarization. The technique has been also applied to CALIPSO

55 aerosol profiles either on selected case studies (Giannakaki et al., 2011) or on a statistical basis (Marinou et al., 2017). In this contribution, we propose a method to determine the extinction coefficient profile using only the elastic and polarization lidar channels at 532 nm. The method has been first suggested by Giannakaki et al. (2017) and further applied by Ansmann et al. (2017). In this contribution, we fully outline the methodology providing an extended sensitivity analysis along with the main advantages and limitations of it. The methodology is limited to cases where only two basic aerosol types are observed

60 and the mixing state of the atmosphere is well known. When the above mention criteria are met, extinction coefficient profiles can be retrieved with non-Raman lidars, even during daytime and with low time resolution windows of 1 hour or less. In case of more complicated aerosol mixture inside the planetary boundary layer, our method is still valid and applicable to free tropospheric aerosol layers.



2 Location and Methodology

65 2.1 Measurement site

CHARADMEExp was an experimental campaign of ESA, implemented by the National Observatory of Athens (NOA), aimed to characterize dust and marine particles along with their mixtures (<http://charadmexp.gr>). The site for the campaign is the monitoring ACTRIS station of Finokalia in Greece as presented in Fig. 1. Finokalia station is located at a remote coastal site in the northeast of the island Crete, Greece, in the Eastern Mediterranean (35.338°N, 25.670°E, 252 asl). The station is located
70 at a top hill, facing the sea within a sector from 270° to 90°. No touristic or other human activities can be found at a distance shorter than 15 km within the aforementioned sector. The site is affected by marine and dust particles by 95% of the time (Mihalopoulos et al., 1997; Kouvarakis et al., 2000). Smoke particles can be advected as well during the August-September forest fire period.

2.3 Models

75 Four-day backward trajectories are calculated using the Hybrid Single-Particle Lagrangian Integrated Trajectory model (HYSPLIT) to gather information about the origin of the observed aerosols and the synoptic patterns corresponding to the measurements. The HYSPLIT 4 model is a complete system for computing simple trajectories to complex dispersion and deposition simulations using either puff or particle approaches. A discussion of the model is given by Draxler and Hess (1997) and Draxler and Hess (1998). The simulations were performed using the GDAS meteorological data. Backward trajectories
80 were computed for several altitudes for the CHARADMEExp campaign period, confirming that the origin of the air masses arriving over our site, were from Saharan region. The BSC-DREAM8b model is additionally used to verify the presence of Saharan dust, indicated from the trajectory analysis. The BSC-DREAM8b model described the desert dust emissions and transport (Nickovic et al., 2001; Pérez et al., 2006; Basart et al., 2012). Moreover, sea salt emissions and transport are described with the atmospheric model RAMS/ICLAMS (Solomos et al., 2011). The model is a further developed version of RAMS 6.0
85 (Pielke et al., 1992) that allows for a fully prognostic treatment of the sea salt particles and their life cycle in the atmosphere. The simulations were used to verify the presence of marine aerosols in the atmosphere during the campaign and specifically during the day under study.

2.2 Description of the lidar system

Polly^{XT} lidar is described by Althausen et al. (2009) and Engelmann et al. (2016). An overview of PollyNET can be found in
90 Baars et al. (2016). Polly^{XT} works with a Nd:YAG laser, emitting pulses at 1064, 532 and 355 nm, with a repetition frequency of 20 Hz. The receiver consists of a Newtonian telescope, with a diameter of 300 mm and a field of view of 1 mrad. Photomultiplier tubes are used for the detection of the elastically backscattered photons at 355, 532 and 1064 nm, as well as for the inelastically backscattered photons at 387 and 607 nm, which correspond to the Raman shift by nitrogen molecules at 355 and 532 nm, respectively. Additionally, the cross-polarized component of radiation at 355 and 532 nm is detected, allowing



95 for the determination of the particle linear depolarization ratio (also called depolarization ratio). In this study, the polarization channels permit us to identify non-spherical dust particles from the near spherical marine aerosols. The Polly^{XT} Arielle system used in this study has been provided by the TROPOS Institute.

The vertical resolution of the signal profiles is 30 m and the raw data are typically stored as 30 s average values. Data were collected on the web page of PollyNET (<http://polly.tropos.de>) where the “quicklooks” of all measurements are available.

100 2.3 Lidar data processing

Lidar data was collected during CHARADMExp campaign (Characterization of Aerosol mixtures of Dust And Marine origin) that took place from the 20th of June 2014 until the 20th of July 2014. The campaign aimed to derive optical, microphysical and chemical properties of marine component and its mixture with dust, employing sophisticated instrumentation. Specifically, aerosol characterization has been established by ground-based active/passive remote sensing techniques, surface in-situ
105 measurements and airborne UAV observations.

For the purposes of this study backscatter coefficient profiles are calculated via Fernald–Klett method (Fernald, 1984; Klett, 1981). The method requires independent information on the lidar ratio and the reference value of the particle backscatter coefficient. Afterwards, the calibrated depolarization ratio profiles at 532 nm, are calculated (Freudenthaler et al. 2009). An overlap correction was applied on the basis of a simple technique proposed by Wandinger and Ansmann (2002). Thus, the aerosol profiles are retrieved down to 500 m. Extinction coefficient profiles at 532 nm are also retrieved based on the Raman
110 method (Ansmann et al., 1992) and are only used for validation purposes of the proposed methodology in this study.

2.4 Elastic Extinction retrieval

A new method, called EIEx [= Elastic Extinction], is proposed for the estimation of extinction coefficient lidar profiles with elastic depolarization lidars. The method makes use of the particle backscatter profiles (β_t) at 532 nm, and the vertically
115 resolved particle linear depolarization ratio measurements (δ_t) at the same wavelength to separate profiles of optical parameters of the marine and dust aerosol types. Values of particle depolarization ratio and lidar ratio of ‘pure’ aerosol types, i.e. Saharan dust and marine, were taken from literature and are presented in Table 1.

Initially, we assume that we don’t have the Polly^{XT} Raman channel. Only later on, Raman extinction retrievals will be used for validation purposes of EIEx. At all stages the signal is screened for clouds, and only cloud free cases are considered. At
120 the first step, we retrieve the backscatter coefficient (β_t) at 532 nm, using an initial lidar ratio of 40 sr, which is a good approximation of dust and marine aerosol mixture. Then, the particle linear depolarization ratio (δ_t), is determined at the same wavelength. If the depolarization ratio is found to be lower than 5 %, the particles are assumed to be marine, and consequently the backscatter retrieval is performed again, using a lidar ratio of 25 sr. In case that the retrieved depolarization ratio found to be larger than 30 %, we assume that the particles are of dust type, and the backscatter retrieval re-performed using a lidar ratio
125 of 55 sr. This value corresponds to pure desert dust particles arriving from Saharan desert. In the majority of our cases, the depolarization ratio is found between 5% and 30 %. In that case, we assume that the probed layer is comprised by an aerosol



130 mixture of dust and marine particles. We separate this mixture to dust and marine backscatter coefficients, based on the methodology proposed by Tesche et al., 2009. The method makes use of vertically resolved particle backscatter and depolarization ratio measurements at the same wavelength, considering the existence of only two aerosol types with well-defined intensive aerosol optical properties. Saharan dust depolarization ratio (δ_d) of 31% and marine depolarization ratio of 5% (δ_m) is assumed for the pure aerosol types (Table 1). The backscatter coefficient of dust and marine aerosols (β_d and β_m) is then converted to extinction profiles by using lidar ratios of 55 sr and 25 sr respectively. The extinction profile is then estimated by the sum of dust and marine extinction profiles. All the input parameters used in this study, are presented in Table 1, and the described methodology is illustrated in Figure 2.

135 3 Results

3.1 CHARADME_{exp} Lidar measurements

140 Range corrected signal (RCS) at 1064 nm as a function of time and height is presented in Figure 3a. The aerosol load inside the Planetary Boundary Layer (PBL) was enhanced throughout the campaign period, while the free tropospheric aerosol load seems to vary with time. Volume depolarization ratio (Fig. 3b) highlight the presence of several depolarizing layers during the campaign, indicating the existence of non-spherical particles. Backward trajectory analysis have confirmed that the origin of these non – spherical particles originates from Saharan region. The Lidar observations show that the dust events developed in the Free Troposphere to end up within the PBL after some days. Thus, RCS within the PBL appears larger after each dust event. Specifically, there are three intense dust events: the first event took place during 17th and 18th of June 2014 at heights up to 5 km. Volume depolarization ratio was maximum during these days with values up to 35%. The second dust event started at noon of 24th of June 2014 in the height of 2 km and within a day the layer has reached up to 5.5 km. This dust event lasted more than 4 days, while several smaller (in terms of intensity) followed. The third dust event started on 5th of July 2014. This dust layer appeared thin with strong volume depolarization ratio and remained thin but not stable in height for almost 3 days. Then this thin layer seemed that expanded up to 6 km. The third event was followed by clouds. The remaining days of the campaign appeared with low volume depolarization ratio indicating almost spherical particles throughout the atmospheric column.

150 3.2 Application to a case study: Dust and marine aerosol mixture

155 We apply the proposed methodology in the measurement performed at the night of 28th of June 2014. The case study was selected based on several criteria: (1) the direction of the air masses indicate dust transport from Saharan region and possible mixture of marine aerosols as well, (2) values of the linear particle depolarization ratio is within 5 and 30 % reveal again possible mixture of dust and marine aerosols, (3) large aerosol load that leads to large SNR which make Raman retrievals possible and (4) the availability of cimel sun-photometric data during that day. Criteria (3) gives us the opportunity to compare



our methodology to concurrent results of extinction profile with the well-established Raman method, while criteria (4) is used to compare our day-time extinction profiles retrieval with an independent instrument.

Four days backward trajectories arriving at Finokalia station on 28th of June 2014 at 02:00 UTC are presented in Figure 4. The trajectories are computed for arrival heights of 500 (red), 2000 (blue) and 4000 m (green) to cover height range of the observed layers that we recognize in coherent structures of height time displays of the range-corrected lidar signal (Figure 3a). The trajectory analysis reveals that is highly possible that the air masses carry marine aerosols at Finokalia station on the day under study, especially in lower heights (500 m arrival height). Trajectory analysis suggest also that dust particles are advected over Finokalia station. Mass concentration profiles performed with RAMS/ICLAMS and DREAM/BSC models are presented in Figure 5 and also confirm the presence of marine aerosol at heights up to 2.5 km and dust particles up to 5 km. Mean sea-salt concentration reach $60 \mu\text{g}/\text{m}^3$ at the first 200 m, decreasing with height. On the contrary the dust mean mass concentrations appear to increase with height, taking the maximum value of $70 \mu\text{g}/\text{m}^3$ at $\sim 1300\text{m}$.

The application of EIEx methodology was performed in 3 hours averaged lidar signals (00:00-03:00 UTC). Backscatter coefficient, using the Klett-Fernald method with initial lidar ratio of 40 sr (Fernald, 1984; Klett, 1981) was retrieved, and is presented in Figure 6 (a) with the black line. A double layer structure was observed; the first layer occurred between 1.4 and 2.8 km and the second one, less intense in terms of aerosol load, between 3 and 5 km. The particle depolarization ratio was measured between 15% and 30%, throughout the atmospheric column, as shown in the same Figure with the green line. The separation of the two aerosol types was applied, and the resolved dust and marine backscatter coefficients are presented in Figure 6 (b). Dust backscatter coefficient, is following the double layer structure, while marine particles contribute less to the total aerosol load. Appropriate lidar ratios were then used, for the estimation of the separated extinction coefficient (see Table 1 and Figure 2), and the estimation of the final retrieval of total extinction coefficient. At the same time frame, Raman extinction coefficient profiles were computed. The results are presented in Figure 6 (c). Comparison between Raman and the proposed methodology shows a very good agreement. In addition, the derived extinction coefficient using the proposed methodology has less noise because is based on the elastic signal. The retrieval of extinction profiles with low temporal resolution is one of the advantage of EIEx methodology.

A small difference is observed between the two extinction coefficient profiles at heights greater than 2.8 km. We believe that the aerosol particles of anthropogenic origin are more probable at these heights, rather than marine aerosols. Anthropogenic aerosols, do not depolarize the light and thus the value of 0.05 that was used fits well for the separation of dust and non-dust particles in general. However, for the retrieval of extinction coefficient profile the aerosol type depended lidar ratio is crucial. Thus, for heights above 2.8 km, a value of 60 sr (Müller at al., 2007) would lead to better comparison with Raman retrievals. The second advantage of EIEx methodology is the ability to check the purity of the non-dust component when Raman retrievals are also available.

A 30 minute average backscatter coefficient analysis has been performed for the whole case day based on Klett-Fernald algorithm, along with the respective particle depolarization retrievals. For validation purposes, we use the aerosol optical depth of level 2, version 3 AERONET sunphotometer data. The total columnar aerosol optical depth, is compared with the lidar-



derived aerosol optical depth, retrieved from integrating the aerosol extinction profiles from 0.5 to 5.5 km. To retrieve the Cimel sunphotometer aerosol optical depth at 532 nm, we use the measured aerosol optical depth at 500 nm and the Ångström exponent between 440 and 870 nm. The results are presented in Figure 7. The results show reasonable agreement between 4 and 10 UTC. There is a noticeable difference between the two datasets after 11 UTC. This is probably due to larger aerosol load in the first 0.5 km, which is not considered in the lidar aerosol optical depth retrieval. This can be seen from the time evolution of the extinction coefficient at the same day presented in Figure 7 (b). The plot shows that after 11 UTC there is enhanced aerosol load between 0.5 and 1 km. Thus, there is indication that the aerosol load could be also enhanced in the lower part of the atmosphere between 0 and 0.5 km. Although the fact that in these height ranges AOD cannot be retrieved due to incomplete overlap, the observed small differences could be attributed to the large aerosol load in the lower boundary layer. The possibility of the retrieval of extinction profiles during day-time with a one-wavelength lidar system is the third advantage of EIEEx methodology.

The quality of the extinction coefficient retrieved by EIEEx is depending on the validity of the assumptions made. Firstly, an appropriate lidar ratio assumption is crucial for the retrieval of a realistic backscatter coefficient. In the case under study the assumption of 40 sr is reasonable taking into account the mixing state of the atmosphere. This is also confirmed by the Raman backscatter coefficient retrieval shown in Figure 8 (b). However, a different assumption of 20 sr (or 60 sr) (which are both extreme values for our case study) will increase (or decrease) the backscatter coefficient at height ranges between 1 and 2 km (Figure 8(a)). The difference would be smaller at higher levels. This assumption will afterwards affect the calculation of the particle depolarization (Figure 6(b)) and thus the contribution of the aerosol types involved (Figure 5). At ranges between 1 and 2 km a lidar ratio of 20 sr will modify the particle depolarization ratio from 25 to 20 %, while a selection of 60 sr will increase the particle depolarization ratio from 25 to 30 %. Thus, the choice of lidar ratio will affect the fraction of marine and dust particles calculated as shown in Figure 5. Changing the lidar ratio from 20 to 60 sr will result on differences of 40% for the contribution for dust particles in the lower part of the atmosphere. The proper selection of depolarization and lidar ratio values for vertical separation have been discussed in previous publications (e.g. Giannakaki et al., 2011, Gross et al., 2011). However, it should be strongly emphasized the critical choice of lidar ratio into the final fraction of the aerosol mixture when Tesche et al., 2008 method is used, especially in cases of elastic lidars.

In our particular case, the assumptions that were made proved to be reasonable, taken into account the trajectory analysis and the values usually observed for marine and dust particles, and thus the comparison with Raman retrievals shows only very small differences (Figure 2(c)). The application of the methodology in more complicated environments is also possible, giving however great attention on the aerosol mixing state and the initial values of the input parameters involved.



4 Conclusions

In this study we present a new method (EiEx) for the estimation of extinction coefficient lidar profiles with elastic depolarization lidars. EiEx make uses of the elastic backscatter coefficient in combination with depolarization ratio in the same wavelength, along with values of depolarization ratio and lidar ratio based on the literature. Reasonable agreement was found, both with Raman retrievals during night time, and with Cimel sunphotometer observations in terms of aerosol optical depth, during day time. This method can be only applied in stations with well-defined aerosol mixtures. There are several advantages of the proposed methodology. Elex is not limited to nighttime Raman observations, and thus is applicable to daytime lidar measurement, with small time period analysis. In case of Raman extinction profiles availability the purity of non-dust component can be additionally checked. In stations with more complicated aerosol mixtures within the planetary boundary layer the methodology is possible to be applied to free tropospheric aerosol layers. CALIPSO extinction retrieval could be also improved when the aerosol mixture is known. However, attention should be given when the separation method is used in elastic backscatter retrievals, regarding not only the depolarization ratio values but also the lidar ratio values selected.

Data Availability

Lidar data is available upon request from the authors and data quicklooks are available on PollyNET website (<http://polly.tropos.de/>). Trajectories are calculated with the NOAA (National Oceanic and Atmospheric Administration) HYSPLIT (HYbrid Single-Particle Lagrangian Integrated Trajectory) model (<https://ready.arl.noaa.gov/HYSPLIT.php>, accessed: 30/04/2019). BSC-DREAM8b model simulations are operated by the Barcelona Supercomputing Center and are available at <https://ess.bsc.es/bsc-dust-daily-forecast/> (accessed: 30/04/2019). RAMS model can be found at <ftp://ftp.mg.uoa.gr/pub/data/iclams1.3.tbz>.

Author contribution

EG developed the methodology and wrote the manuscript. EG, PK and EM performed the lidar data analysis. NB analyzed the model simulations. VA and AA initiated the measurement campaign. All authors participated in scientific discussions on this study and reviewed/edited the manuscript during its preparation process.

Competing interests

The authors declare that they have no conflict of interest.



Acknowledgments

250 Elina Giannakaki acknowledges the support of the Academy of Finland (project no. 270108). BSC-DREAM8b simulations were performed on the Mare Nostrum supercomputer hosted by the Barcelona Supercomputing Center-Centro Nacional de Supercomputación (BSC).

255



References

- Althausen, D., Engelmann, R., Baars, H., Heese, B., Ansmann, A., and Müller, M.: Portable Raman lidar PollyXT for automated profiling of aerosol backscatter, extinction, and depolarization, *J. Atmos. Oceanic Technol.*, 26, 2366–2378, doi:10.1175/2009JTECHA1304.1, 2009.
- 260 Amiridis, V., Balis, D. S., Kazadzis, S., Bais, A., Giannakaki, E., Papayannis, A., and Zerefos, C.: Four-year aerosol observations with a Raman lidar at Thessaloniki, Greece, in the framework of European Aerosol Research Lidar Network (EARLINET), *J. Geophys. Res.*, 110, D21203, doi:10.1029/2005JD006190, 2005.
- Ansmann, A., Wandinger, U., Riebesell, M., Weitkamp, C., and Michaelis, W.: Independent measurement of extinction and backscatter profiles in cirrus clouds by using a combined Raman elastic-backscatter lidar, *Appl. Opt.*, 31, 7113–7131, 1992.
- 265 Ansmann, A., Wagner, F., Müller, D., Althausen, D., Herber, A., von Hoyningen-Huene, W., and Wandinger, U.: European pollution outbreaks during ACE 2: Optical particle properties inferred from multiwavelength lidar and star-Sun photometry, *J. Geophys. Res.*, 107(D15), 4259, doi:10.1029/2001JD001109, 2002.
- Ansmann, A., Rittmeister, F., Engelmann, R., Basart, S., Jorba, O., Spyrou, C., Remy, S., Skupin, A., Baars, H., Seifert, P., Senf, F., and Kanitz, T.: Profiling of Saharan dust from the Caribbean to western Africa – Part 2: Shipborne lidar measurements versus forecasts, *Atmos. Chem. Phys.*, 17, 14987–15006, <https://doi.org/10.5194/acp-17-14987-2017>, 2017.
- 270 Baars, H., Kanitz, T., Engelmann, R., Althausen, D., Heese, B., Komppula, M., Preißler, J., Tesche, M., Ansmann, A., Wandinger, U., Lim, J.-H., Ahn, J. Y., Stachlewska, I. S., Amiridis, V., Marinou, E., Seifert, P., Hofer, J., Skupin, A., Schneider, F., Bohlmann, S., Foth, A., Bley, S., Pfüller, A., Giannakaki, E., Lihavainen, H., Viisanen, Y., Hooda, R. K., Pereira, S., Bortoli, D., Wagner, F., Mattis, I., Janicka, L., Markowicz, K. M., Achtert, P., Artaxo, P., Pauliquevis, T., Souza, R. A. F., Sharma, V. P., van Zyl, P. G., Beukes, J. P., Sun, J., Rohwer, E. G., Deng, R., Mamouri, R. E., and Zamorano, F.: An overview of the first decade of PollyNET: an emerging network of automated Raman-polarization lidars for continuous aerosol profiling, *Atmos. Chem. Phys.*, 16, 5111–5137, doi:10.5194/acp-16-5111-2016, 2016.
- 275 Balis, D. S., Amiridis, V., Zerefos, C., Kazantzidis, A., Kazadzis, S., Bais, A. F., Meleti, C., Gerasopoulos, E., Papayannis, A., Matthias, V., Dier, H., and Andreae, M. O.: Study of the effect of different type of aerosols on UV-B radiation from measurements during EARLINET, *Atmos. Chem. Phys.*, 4, 307–321, doi:10.5194/acp-4-307-2004, 2004.
- 280 Basart, S., Pérez, C., Nickovic, S., Cuevas, E., and Baldasano, J. M.: Development and evaluation of the BSC-DREAM8Bb dust regional model over Northern Africa, the Mediterranean and the Middle East, *Tellus B*, 64, doi:10.3402/tellusb.v64i0.18539, 2012.
- Dawson, K. W., Meskhidze, N., Josset, D., and Gassó, S.: Spaceborne observations of the lidar ratio of marine aerosols, *Atmos. Chem. Phys.*, 15, 3241–3255, doi:10.5194/acp-15-3241-2015, 2015.
- 285 Draxler, R. R. and Hess, G. D.: Description of the HYSPLIT 4 modeling system, NOAA Tech Memo, ERL ARL-224, NOAA, Silver Spring, Md, 1997.



- Draxler, R. R. and Hess, G. D.: An overview of the HYSPLIT 4 modelling system for trajectories, dispersion and deposition, *Australian Meteorological Magazine*, 47, 1998.
- 290 Engelmann, R., Kanitz, T., Baars, H., Heese, B., Althausen, D., Skupin, A., Wandinger, U., Komppula, M., Stachlewska, I. S., Amiridis, V., Marinou, E., Mattis, I., Linné, H., and Ansmann, A.: The automated multiwavelength Raman polarization and water-vapor lidar PollyXT: the neXT generation, *Atmos. Meas. Tech.*, 9, 1767-1784, doi:10.5194/amt-9-1767-2016, 2016.
- Fernald, F. G.: Analysis of atmospheric lidar observations: some comments, *Appl. Opt.* 23, 652-653, https://doi.org/10.1364/AO.23.000652, 1984.
- 295 Freudenthaler, V., Esselborn, M., Wiegner, M., Heese, B., Tesche, M., Ansmann, A., Müller, D., Althausen, D., Wirth, M., Fix, A., Ehret, G., Knippertz, P., Toledano, C., Gasteiger, J., Garhammer, M., and Seefeldner M.: Depolarization ratio profiling at several wavelengths in pure Saharan dust during SAMUM 2006, *Tellus B*, 61, 165–179, doi:10.1111/j.1600-0889.2008.00396.x, 2009.
- Giannakaki, E., Balis, D. S., Amiridis, V., and Zerefos, C: Optical properties of different aerosol types: seven years of combined Raman-elastic backscatter lidar measurements in Thessaloniki, Greece, *Atmos. Meas. Tech.*, 3, 569–578, doi:10.5194/amt-3-569-2010, 2010.
- 300 Giannakaki, E., van Zyl, P. G., Müller, D., Balis, D., and Komppula, M.: Optical and microphysical characterization of aerosol layers over South Africa by means of multi-wavelength depolarization and Raman lidar measurements, *Atmos. Chem. Phys.*, 16, 8109-8123, doi: 10.5194/acp-16-8109-2016, 2016.
- 305 Giannakaki, E., Balis, D., and Amiridis, V.: Vertical resolved separation of aerosol types using CALIPSO level-2 product, *Proc. SPIE 8182, Lidar Technologies, Techniques, and Measurements for Atmospheric Remote Sensing VII*, 81820T, doi: 10.1117/12.898095, 2011.
- Giannakaki, E., Kokkalis, P., Marinou, E., Solomos, S., Amiridis, V., Ansmann, A., Bartsotas, N., Engelmann, R., and Komppula, M.: Extinction profile retrieval at Finokalia, Crete, in the proceedings of 28th International Laser and Radar
- 310 Conference, Bucharest, Romania, 2017.
- Groß, S, Tesche, M., Freudenthaler, V., Toledano, C., Wiegner, M., Ansmann, A., Althausen, D., and Seefeldner, M.: Characterization of Saharan dust, marine aerosols and mixtures of biomass-burning aerosols and dust by means of multi-wavelength depolarization and Raman lidar measurements during SAMUM 2, *Tellus B.: Chemical and Physical Meteorology*, 63, 2011.
- 315 Groß, S, Esselborn, M., Weinzierl, B., Wirth, M., Fix, A., and Petzld, A.: Aerosol classification by airborne high spectral resolution lidar observations, *Atmos. Chem. Phys.*, 13, 2487 – 2505, 2013.
- Groß, S, Freudenthaler, V., Schepanski, K., Toledano, C., Schäfler, A., Ansmann, A., and Weinzierl, B.: Optical properties of long-range transported Saharan dust over Barbados as measured by dual-wavelength depolarization Raman lidar measurements, *Atmos. Chem. Phys.*, 15, 11067-11080, 2015.
- 320 IPCC, Climate Change 2013: The Physical Science Basis. Contribution of Working Group I to the Fifth Assessment Report of the Intergovernmental Panel on Climate Change [Stocker, T.F., D. Qin, G.-K. Plattner, M. Tignor, S.K. Allen, J. Boschung,



- A. Nauels, Y. Xia, V. Bex and P.M. Midgley (eds.)]. Cambridge University Press, Cambridge, United Kingdom and New York, NY, USA, doi:10.1017/CBO9781107415324, 2013.
- 325 Kaufman, Y. J., Tanre, D., and Boucher, O.: A satellite view of aerosols in the climate system, *Nature*, 419, doi:10.1038/nature01091, 2002.
- Kouvarakis, G., Tsigaridis, K., Kanakidou, M., Michalopoulos, N., Temporal variations of surface regional background ozone over Crete Island in the southeast Mediterranean, *J. Geophys. Res.*, 105, 2000.
- Klett, J. D.: Stable analytical inversion solution for processing lidar returns, *Appl. Opt.* 20, 211-220, <https://doi.org/10.1364/AO.20.000211>, 1981.
- 330 Mamouri, R.E., and Ansmann, A.: Fine and coarse dust separation with polarization lidar, *Atmos. Meas. Tech.*, 7, 3717–3735, doi:10.5194/amt-7-3717-2014, 2014.
- Marinou, E. , Amiridis, V., Binietoglou, I., Tsiakerdekis, A. , Solomos, S., Proestakis, E., Konsta, D., Papagiannopoulos, N., Tsekeri, A., Vlastou, G., Zanis, P., Balis, D., Wandinger, U., and Ansmann, A.: Three-dimensional evolution of Saharan dust transport towards Europe based on a 9-year EARLINET-optimized CALIPSO dataset, *Atmos. Chem. Phys.*, 17, 5893–5919, doi:10.5194/acp-17-5893-2017, 2017.
- 335 Mattis, I., Ansmann, A., Müller, D., Wandinger, U., and Althausen, D.: Multiyear aerosol observations with dual-wavelength Raman lidar in the framework of EARLINET, *J. Geophys. Res.*, 109, D13203, doi:10.1029/2004JD004600, 2004.
- Mona, L., Amodeo, A., Pandolfi, M., and Pappalardo, G.: Saharan dust intrusions in the Mediterranean area: Three years of Raman lidar measurements, *J. Geophys. Res.*, 111, D16203, doi:10.1029/2005JD006569, 2006.
- 340 Müller, D., Ansmann, A., Mattis, I., Tesche, M., Wandinger, U., Althausen, D. and Pisani, G.: Aerosol-type-dependent lidar ratios observed with Raman lidar, *J. Geophys. Res.*, 112, D16202, doi:10.1029/2006JD008292, 2007.
- Papayannis, A., Amiridis, V., Mona, L., Tsaknakis, G., Balis, D., Bösenberg, J., Chaikovski, A., De Tomasi, F., Grigorov, I., Mattis, I., Mitev, V., Müller, D., Nickovic, S., Perez, C., Pietruczuk, A., Pisani, G., Ravetta, F., Rizi, V., Sicard, M., Trickl, T., Wiegner, M., Gerding, M., Mamouri, R. E., D’Amico, G. and Pappalardo, G.: Systematic lidar observations of Saharan dust over Europe in the frame of EARLINET (2000–2002), *J. of Geophys. Res.: Atm.*, American Geophysical Union, 113 (D10), D10204, 2008.
- 345 Mihalopoulos, N., Stephanou, E., Kanakidou, M., Pilitsidis, S., and Bousquet, Tropospheric aerosol ionic composition above Eastern Mediterranean area, *Tellus*, 49B, 1997.
- Nickovic, S., Kallos, G., Papadopoulos, A. and Kakaliagou, O.: A model for prediction of desert dust cycle in the atmosphere, *J. Geophysical Res.*, 106, D16, 2001.
- 350 Papayannis, A., Balis, D., Amiridis, V., Chourdakis, G., Tsaknakis, G., Zerefos, C., Castanho, A. D. A., Nickovic, S., Kazadzis, S., and J. Grabowski: Measurements of Saharan dust aerosols over the Eastern Mediterranean using elastic backscatter-Raman lidar, spectrophotometric and satellite observations in the frame of the EARLINET project, *Atmos. Chem. Phys.*, 5, 2065-2079, doi:10.5194/acp-5-2065-2005, 2005.



- 355 Pérez, C., Nickovic, S., Pejanovic, G., Baldasano, J. M. & Özsoy, E., 2006b: Interactive dust-radiation modeling: A step to improve weather forecasts, *J. Geophys. Res.*, 111, D16206, doi: 10.1029/2005JD006717, 2006.
- Pielke, R. A., Cotton, W. R., Walko, R. L., Tremback, C. J., Lyons, W. A., Grasso, L. D., Nicholls, M. E., Moran, M. D., Wesley, D. A., Lee, T. J. and Copeland, J. H.: 1992, A Comprehensive Meteorological Modeling System RAMS, *Meteorol. Atmos. Phys.* 49, 1992.
- 360 Solomos, S., Kallos, G., Kushta, J., Astitha, M., Tremback, C., Nenes, A., and Levin, Z., An integrated modeling study on the effects of mineral dust and sea salt particles on clouds and precipitation, *Atmos. Chem. Phys.*, 11, 873-892, 2011
<https://doi.org/10.5194/acp-11-873-2011>.
- Tesche, M., Ansmann, A., Müller, D., Althausen, D., Engelmann, R., Freudenthaler, V., and Groß, S.: Vertically resolved separation of dust and smoke over Cape Verde by using multiwavelength Raman and polarization lidars during Saharan
- 365 Mineral Dust Experiment 2008, *J. Geophys. Res.*, 114, D13202, doi:10.1029/2009JD011862, 2009.
- Wandinger, U. and Ansmann, A.: Experimental determination of the lidar overlap profile with Raman lidar, *Appl. Optics*, 41, 511–514, 2002.



370

Figures

375

380

385

390

395



400 **Figure 1.** Location of Finokalia Station (red dot) in Crete, Greece.

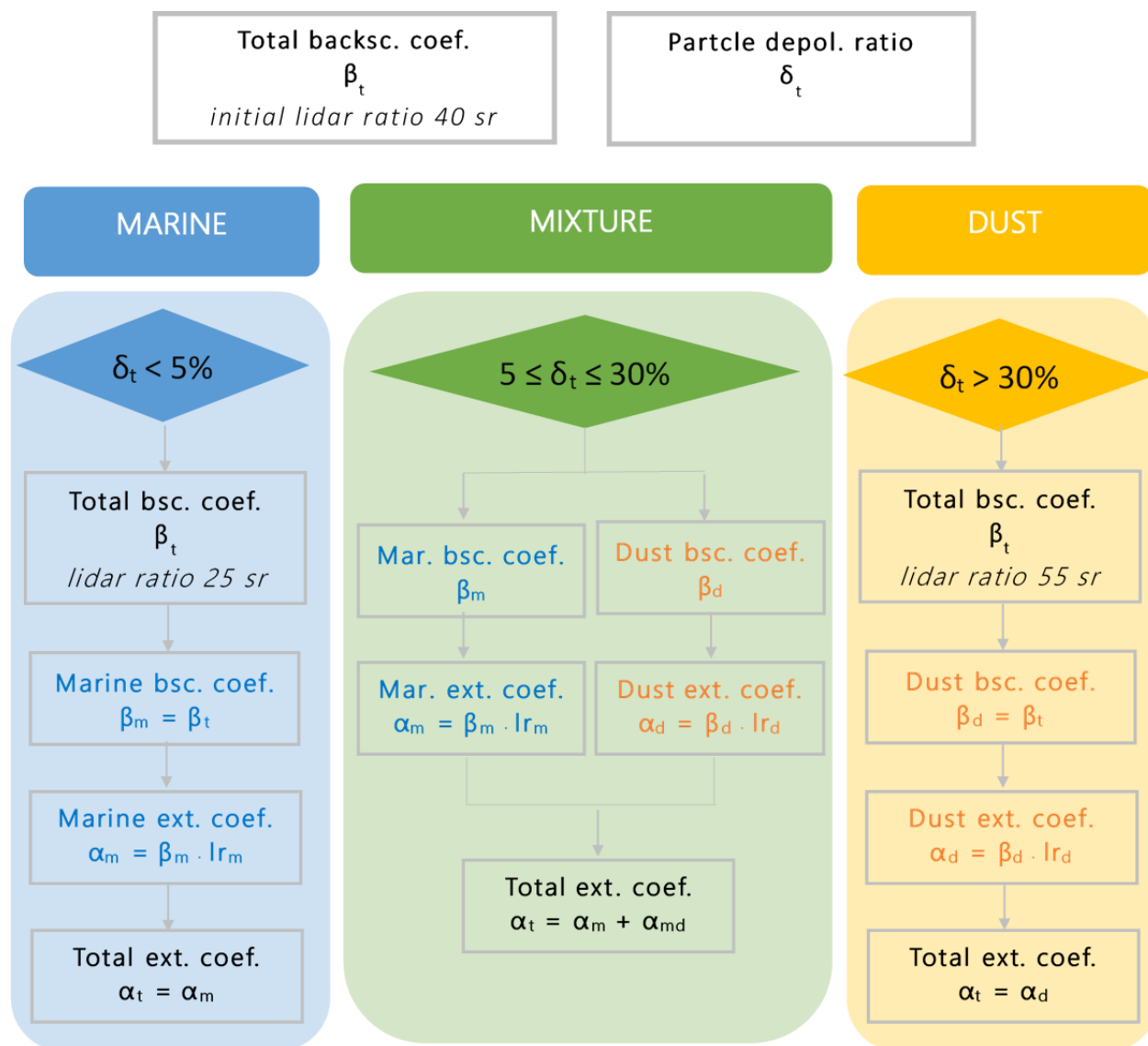


Figure 2 Flowchart of the proposed methodology for the retrieval of extinction coefficient profile using backscatter and depolarization data.

405

410



415

420

425

430

435

440

445

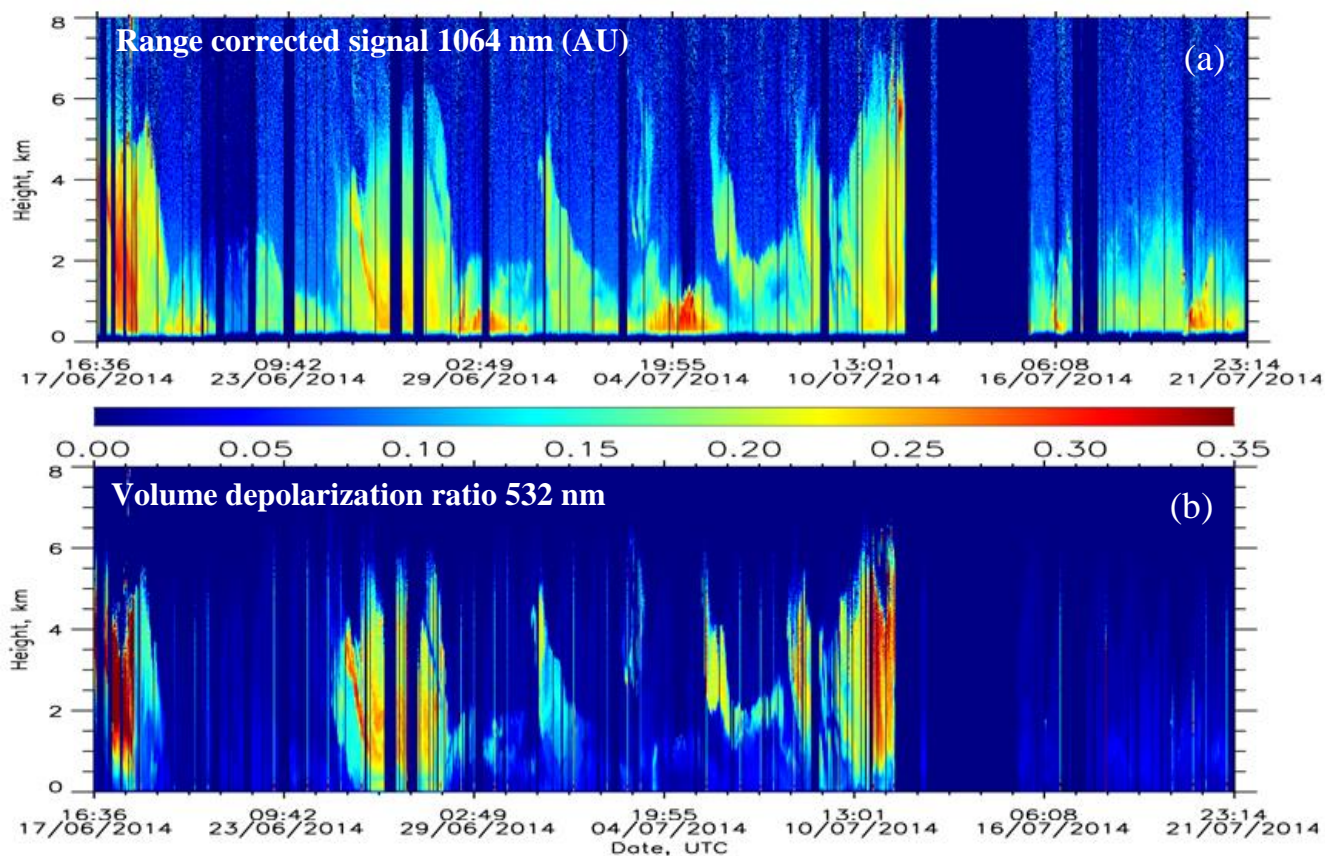


Figure 3 Range corrected signal at 1064 nm (a) and volume depolarization ratio (b) at Finokalia during CHARADME campaign.



NOAA HYSPLIT MODEL
Backward trajectories ending at 0200 UTC 28 Jun 14
GDAS Meteorological Data

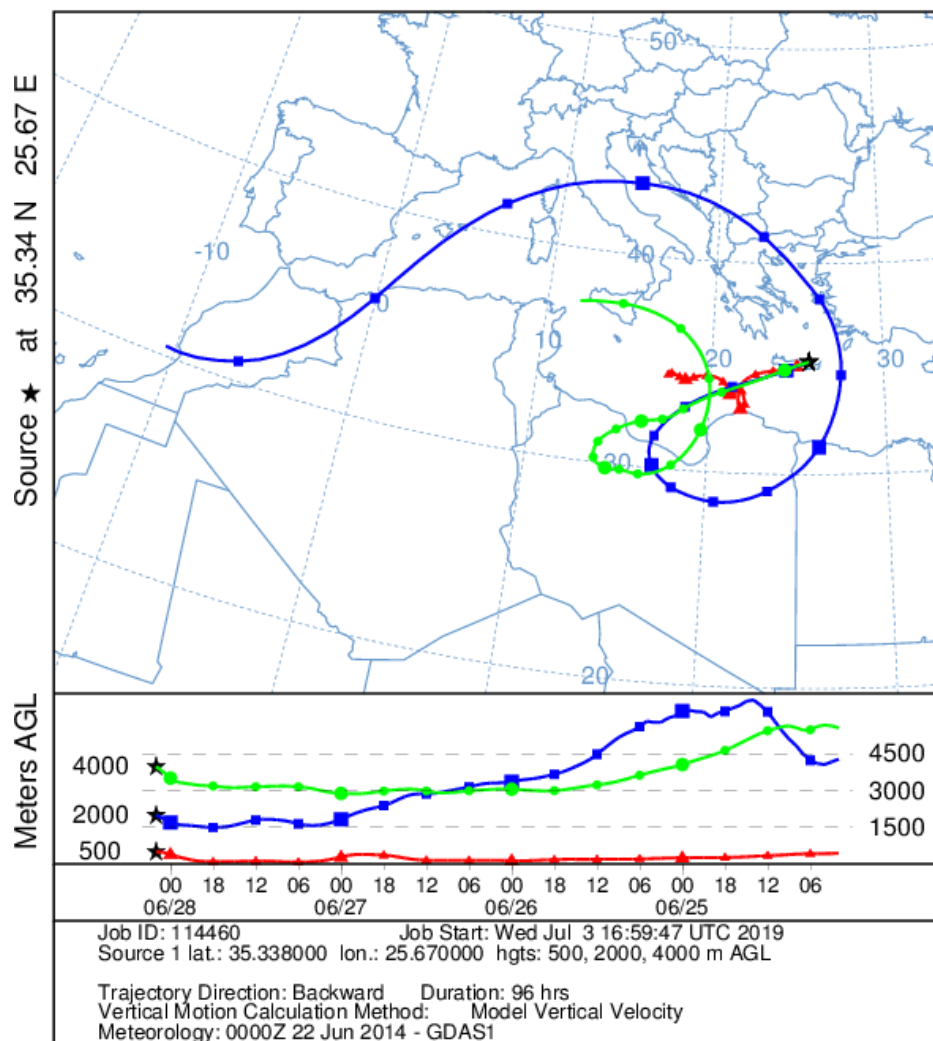


Figure 4. Four days backward trajectories at 02:00 UTC on 28th June 2014 at Finokalia, Crete. The arrival heights are set to 500, 1000 and 4000 m.

450

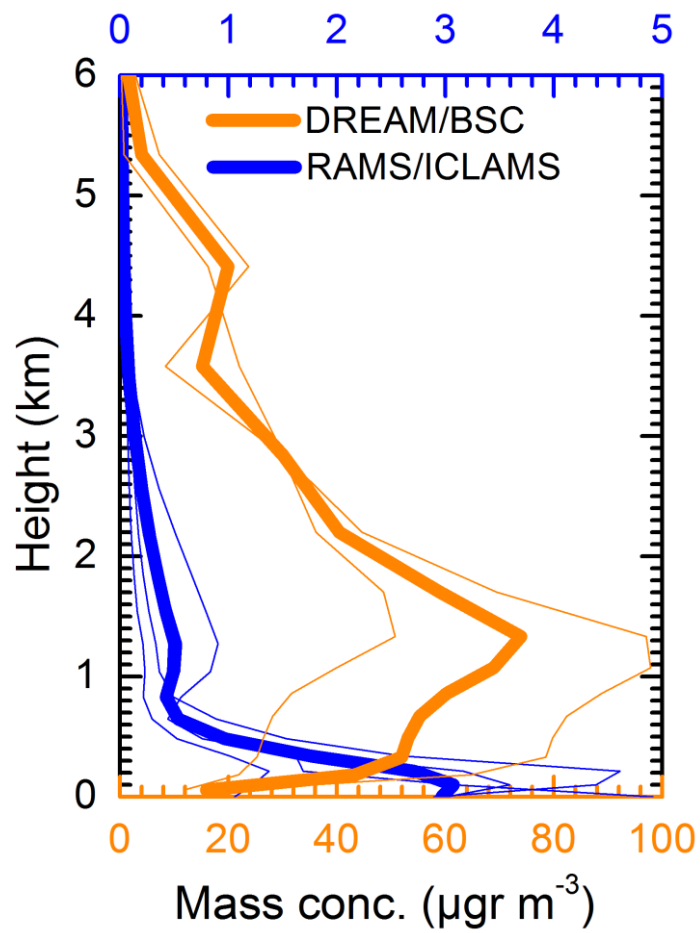


Figure 5. Simulations of sea-salt (blue) and dust (orange) mass concentrations profiles using RAMS/ICLAMS and DREAM/BSC models for 28th of June 2014, 00:00-03:00 UTC.

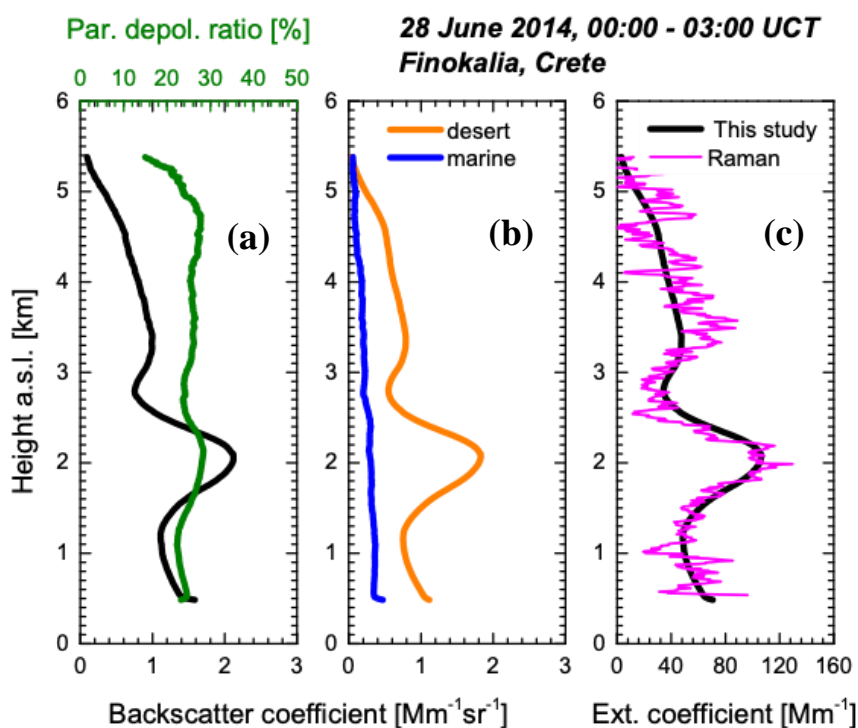
455



460

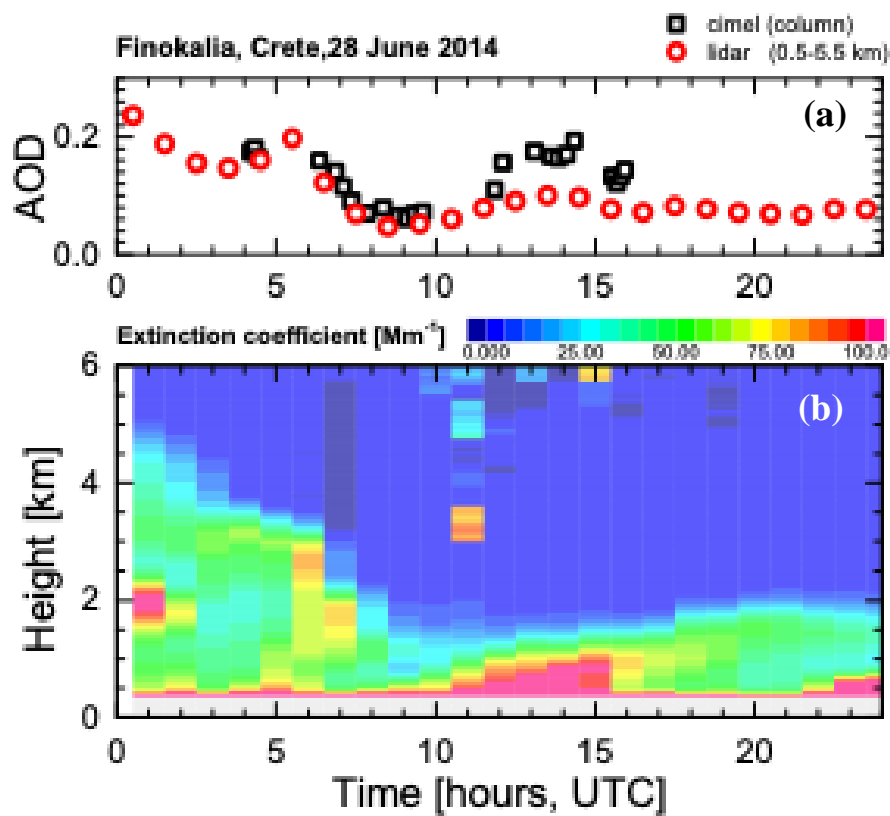
465

470



475

Figure 6: (a) Backscatter coefficient (black) and particle depolarization ratio (green) at 532nm for 28th of June 2014, 00:00-03:00 UTC. (b) Backscatter coefficient for desert dust (orange) and marine (blue) particles. (c) Extinction coefficient at 532 nm with the proposed method (black) and using the standard Raman retrieval (pink).



480 Figure 7. Time series of the aerosol optical depth at 532 nm from sun photometric data (total column) and from lidar retrieval (0.5-5.5 km). Color plot of the extinction coefficient for 28th of June 2014.



485

490

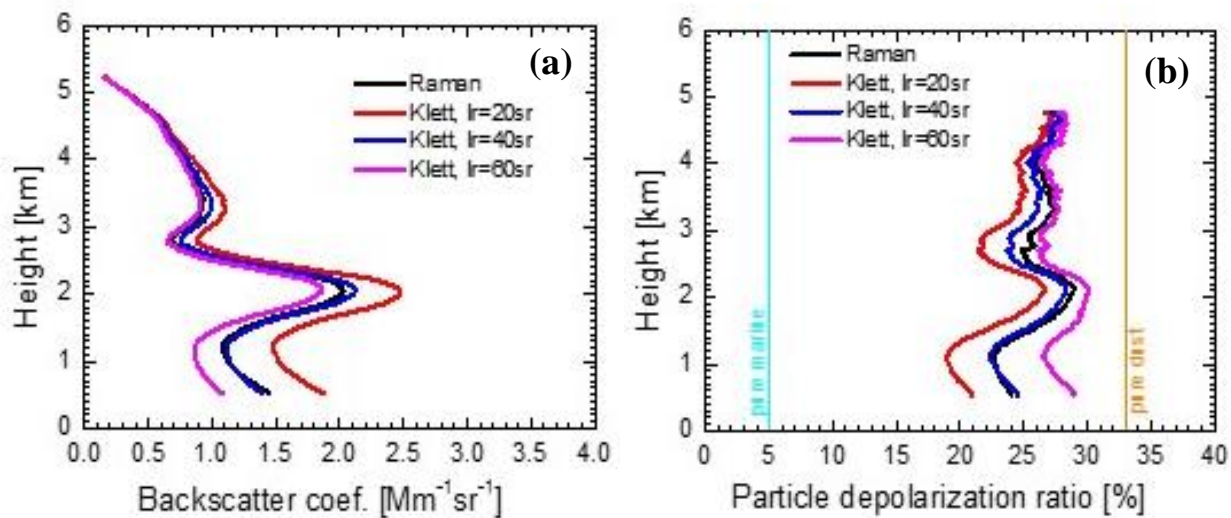
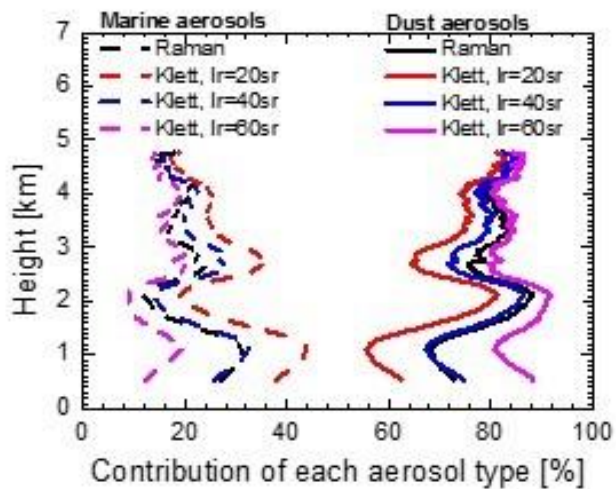


Figure 8. (a) The backscatter coefficient for different lidar ratio initial values for Klett and Raman retrieval and (b) the corresponding particle depolarization ratio profiles.

495



510 **Figure 9.** Fraction of marine (dotted) and dust (solid) aerosols based on lidar ratio selection on Klett retrieval and the fraction calculated based on the Raman based technique (black).



515 Tables

Table 1. Overview of the input parameters used in our study.

| Parameter | Aerosol Type | Symbol | Value | Reference |
|-----------------------------------------|--------------|------------|-------|------------------------------------------------------------------------------------------------------------------------------------------|
| Lidar ratio at 532 nm | Marine | lr_m | 25 sr | Müller et al., 2007; Dawson et al. 2015; Gross et al. 2011; Gross et al. 2013, Gross et al. 2015 |
| | Saharan dust | lr_d | 55 sr | Mattis et al. 2002; Mona et al. 2006; Papayannis et al. 2005; Balis et al. 2004, Gross et al. 2011; Gross et al. 2013, Gross et al. 2015 |
| Particle depolarization ratio at 532 nm | Marine | δ_m | 0.05 | Gross et al. 2011; Gross et al. 2013, Gross et al. 2015 |
| | Saharan dust | δ_d | 0.31 | Freudenthaler et al. (2009); Gross et al. 2011; Gross et al. 2013, Gross et al. 2015 |